Proceedings of
2003 ASME Summer Heat Transfer Conference
July 21–23, 2003, Las Vegas, Nevada, USA

HT2003-47233

DEPENDENT SCATTERING AND FIELD ENHANCEMENT IN MONOCHROMATIC IRRADIATED, RANDOM POROUS MEDIA

X.L. Ruan and M. Kaviany*
Department of Mechanical Engineering, University of Michigan, Ann Arbor, MI 48109-2125

ABSTRACT
Solving the Maxwell's equations, an electric filed enhancement is observed in monochromatically irradiated, one- and two-dimensional dispersed dielectric solids with random size distribution. This enhancement is a few orders of magnitude higher than the incident field, for some arrangements. The probability density and the location of enhanced field are determined forgiven solid complex refractive index and particle size distribution. Using the two-flux model, the equation of radiative heat transfer (ERT) is solved for the local intensity. It is shown that ERT can represent a statistical average behavior of the intensity (by introducing corrections to the scattering and absorption coefficients based on dependent scattering). However, ERT is not suitable for predicting field enhancement and photon localization.
Keywords: field enhancement, dependent scattering, photon localization, porous media

NOMENCLATURE
d_s = solid particle size, nm
E = complex electric field, V/m
I = intensity, W/m^2
k = wave number, m^{-1}
m = complex refractive index
n = refractive index
$\dot{s}$ = volumetric energy conversion, W/m^3
T = transmission

Greek symbol
ε = porosity
ε_0 = free space electric permittivity, F/m
ε_e = relative electric permittivity
κ = extinction index
μ_0 = free space permeability, H/m
μ_e = relative permeability
λ = wavelength, nm
θ = scattering angle
σ = coefficient
Φ = scattering phase function

Subscript
a = absorption
e = extinction
f = fluid
i = incident
r = reflected
s = solid, scattering
t = transmitted

Superscript
* = dimensionless quantity
\+ = forward
\- = backward

INTRODUCTION
Radiation heat transfer in disordered porous media includes prescribed irradiation as well as internal emission. The infrared irradiation of compacts of dielectric, random poly-sized nano-particles has been used for up-conversion lasing (absorption and then emission at higher frequencies and lower wavelengths, including those in the visible portion of the spectrum) [1, 2]. Irradiation of powders has also been used in nano-manufacturing. Traditionally, porous media are treated as a single continuum with effective properties using the equation of radiative transfer (ERT) [3]. The effective properties are derived from the spectral radiative behavior of a single isolated particle, using large and small particle size approximations, and by inclusion of some inter-particle interactions (dependent scattering). The local radiative intensity in the medium is determined using ERT.

While the theory of dependent scattering allows for coherent superposition and a local enhancement of the electromagnetic field (the so-called Anderson localization

* Corresponding author, kaviany@umich.edu

characterized by a mean-free path on the order of the particle size) [4-6], the existing effective property treatments are not capable of capturing this phenomenon. In this study, using one- and two-dimensional dispersed solids with random size distributions, and using the Maxwell's equations, the propagation of electromagnetic (EM) waves and local field enhancement are determined. The results show field enhancement of a few orders of magnitude higher than the incidence in some random arrangements, and the associated photon localization. It is then shown that ERT, by introducing corrections to the scattering and absorption coefficients based on dependent scattering, represents a statistical average behavior of the EM treatment. So ERT is not suitable for the prediction of this localization.

1. ONE-DIMENSIONAL GEOMETRY

1.1 Formulation and Solution Procedure

The simplest model of a random porous medium consists of parallel solid layers with random thickness, as shown in Fig. 1. This multilayer medium has a finite length in the direction of the electromagnetic wave propagation *x,* and an infinite length in the plane normal to *x*. It can thus be treated as a one-dimensional system. The dielectric solid material has a complex refractive index m_s ($= n_s - i\kappa_s$), while the fluid is assumed to be air and has a real refractive index m_f ($= n_f = 1$).

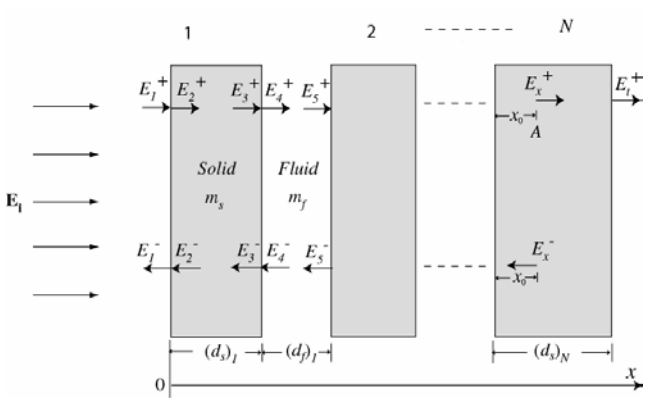

Fig. 1. Parallel solid layers with random thickness. The fluid layer thickness is also random. The porosity is prescribed.

The transfer matrix method [7] is used for the solution of the Maxwell's equations in this multilayer medium, subject to a uniform normal incident field. The field in the medium can be divided into two components, the forward (transmitted) component E^+ and the backward (reflected) component E^-, also shown in Fig.1. The components at the interface of two different media with the refractive indices m_s and m_f are related by the transfer matrix

$$\begin{bmatrix} E_1^+ \\ E_1^- \end{bmatrix} = \begin{bmatrix} \dfrac{m_s+m_f}{2m_f} & \dfrac{m_s-m_f}{2m_f} \\ \dfrac{m_s-m_f}{2m_f} & \dfrac{m_s+m_f}{2m_f} \end{bmatrix} \begin{bmatrix} E_2^+ \\ E_2^- \end{bmatrix} . \tag{1}$$

The components within the same layer are related by the transfer matrix

$$\begin{bmatrix} E_2^+ \\ E_2^- \end{bmatrix} = \begin{bmatrix} e^{ik_s(d_s)_1} & 0 \\ 0 & e^{-ik_s(d_s)_1} \end{bmatrix} \begin{bmatrix} E_3^+ \\ E_3^- \end{bmatrix}, \tag{2}$$

where k_s ($= 2\pi/\lambda_s$) is the wave number, and λ_s is the wavelength in solids. Equations (1) and (2) are repeated for all layers. If trace all *N* layers, the field at the first and the last boundaries are related through

$$\begin{bmatrix} E_1^+ \\ E_1^- \end{bmatrix} = \left[\prod_{j=1}^{N-1} \left(M_{s,j} M_{f,j} \right) \right] M_{s,N} \begin{bmatrix} \dfrac{m_f+m_s}{2m_s} & \dfrac{m_f-m_s}{2m_s} \\ \dfrac{m_f-m_s}{2m_s} & \dfrac{m_f+m_s}{2m_s} \end{bmatrix} \begin{bmatrix} E_t^+ \\ 0 \end{bmatrix} , \tag{3}$$

where

$$M_{s,j} = \begin{bmatrix} \dfrac{m_s+m_f}{2m_f} & \dfrac{m_s-m_f}{2m_f} \\ \dfrac{m_s-m_f}{2m_f} & \dfrac{m_s+m_f}{2m_f} \end{bmatrix} \begin{bmatrix} e^{ik_s(d_s)_j} & 0 \\ 0 & e^{-ik_s(d_s)_j} \end{bmatrix} \tag{4}$$

and

$$M_{f,j} = \begin{bmatrix} \dfrac{m_f+m_s}{2m_s} & \dfrac{m_f-m_s}{2m_s} \\ \dfrac{m_f-m_s}{2m_s} & \dfrac{m_f+m_s}{2m_s} \end{bmatrix} \begin{bmatrix} e^{ik_f(d_f)_j} & 0 \\ 0 & e^{-ik_f(d_f)_j} \end{bmatrix} . \tag{5}$$

Given the incident field E_1^+ ($= E_i$), the reflected field E_1^- ($= E_r$) and transmitted field E_t^+ are found from Eq. (3). Once the reflected field component E_1^- has been solved successfully, the next stage in the calculation is to obtain the electric field at a large collection of points in the medium. Similarly, for an arbitrary location A, which lies in the *M*-th layer, with the coordinate x_0 from the layer surface and *x* from the medium surface (Fig. 1), the field is related to the first layer by

$$\begin{bmatrix} E_1^+ \\ E_1^- \end{bmatrix} = \left[\prod_{j=1}^{M-1} \left(M_{s,j} M_{f,j} \right) \right] \begin{bmatrix} \dfrac{m_s+m_f}{2m_f} & \dfrac{m_s-m_f}{2m_f} \\ \dfrac{m_s-m_f}{2m_f} & \dfrac{m_s+m_f}{2m_f} \end{bmatrix} \begin{bmatrix} e^{ik_s x_0} & 0 \\ 0 & e^{-ik_s x_0} \end{bmatrix} \begin{bmatrix} E_x^+ \\ E_x^- \end{bmatrix} \tag{6}$$

Then the magnitude of the local field is given by

$$|E| = \left| E_x^+ + E_x^- \right| \tag{7}$$

Thus the local intensity *I* and volumetric heat generation $\dot{s}$ become [8]

$$I = \frac{1}{2}|E|^2 \operatorname{Re}\left(\sqrt{\frac{\varepsilon_0 \varepsilon_e}{\mu_0 \mu_e}} \right) = \frac{1}{2} n \sqrt{\frac{\varepsilon_0}{\mu_0}} |E|^2 \tag{8}$$

and

$$\dot{s} = \sigma_a I = \frac{4\pi\kappa_s}{\lambda} I \ , \tag{9}$$

where μ_0 is the free space permeability, μ_e (=1 here) is the relative permeability, ε_0 is the free space permittivity, ε_e is the relative permittivity related to the complex refractive index m by $\varepsilon_e = m^2$. Re( ) means the real part of a complex number, and σ_a is the absorption coefficient.

1.2 Results and Discussions

1.2.1 Field Enhancement Phenomenon

The local electric field is determined for a normal incident electromagnetic wave of wavelength λ = 1000 nm, for the one-dimensional random media with 50 solid layers whose thickness d_s is a random number between $<d_s> \pm \Delta d_s$ = 1000±800 nm, and with the porosity $\varepsilon = 0.35$, $n_s = 1.8$ and $\kappa_s = 10^{-5}$ (n_s and κ_s are for doped yttria compacts [1]). There are infinite possible realizations for this model composite, and the field results for one of them are shown in Figs. 2(a) to (d), where the dimensionless parameters are defined as follows: $|E|^* = |E|/|E_i|$, $I^* = I/I_i$ and $\dot{s}^* = \dot{s} < d_s > / I_i$.

It is shown in Fig. 2(a) that there is a field enhancement, i.e., there is a peak inside the medium and this peak can be several times larger than the incident field. Note that in periodic porous media, the field is also periodic, resulting in no isolated peaks inside the media (even if the field in this case can also be higher than the incident field). The same peak in the intensity is shown in Fig. 2(b). Note that, using the continuous medium approximation, which is adopted in ERT, there will be no peaks, but an exponential decay of the intensity (due to absorption and scattering, since no emission is considered here). As shown in Fig. 2(c), the volumetric heat generation $\dot{s}$ due to absorption also has a peak within the medium. Fig. 2(d) is obtained by averaging the intensities inside each layer, and therefore, also represents the distribution of the solid layers for this realization. As can be seen, the highest $\dot{s}$ occurs at the 25th layer from the surface, indicating a large volumetric absorption rate. From the optics viewpoint, the peak is where the photons are localized and "stored", and where the absorption is the most significant. Photon localization was also examined by a transmission approach [9, 10], but they gave the bulk transmission coefficients, unlike the enhanced local field given here.

Note that field enhancement is based on the electromagnetic field coherence. Thus, the coherence condition (the medium size is smaller than the coherence length) must be satisfied to observe field enhancement. The coherence length is $\lambda^2/\Delta\lambda$ for a

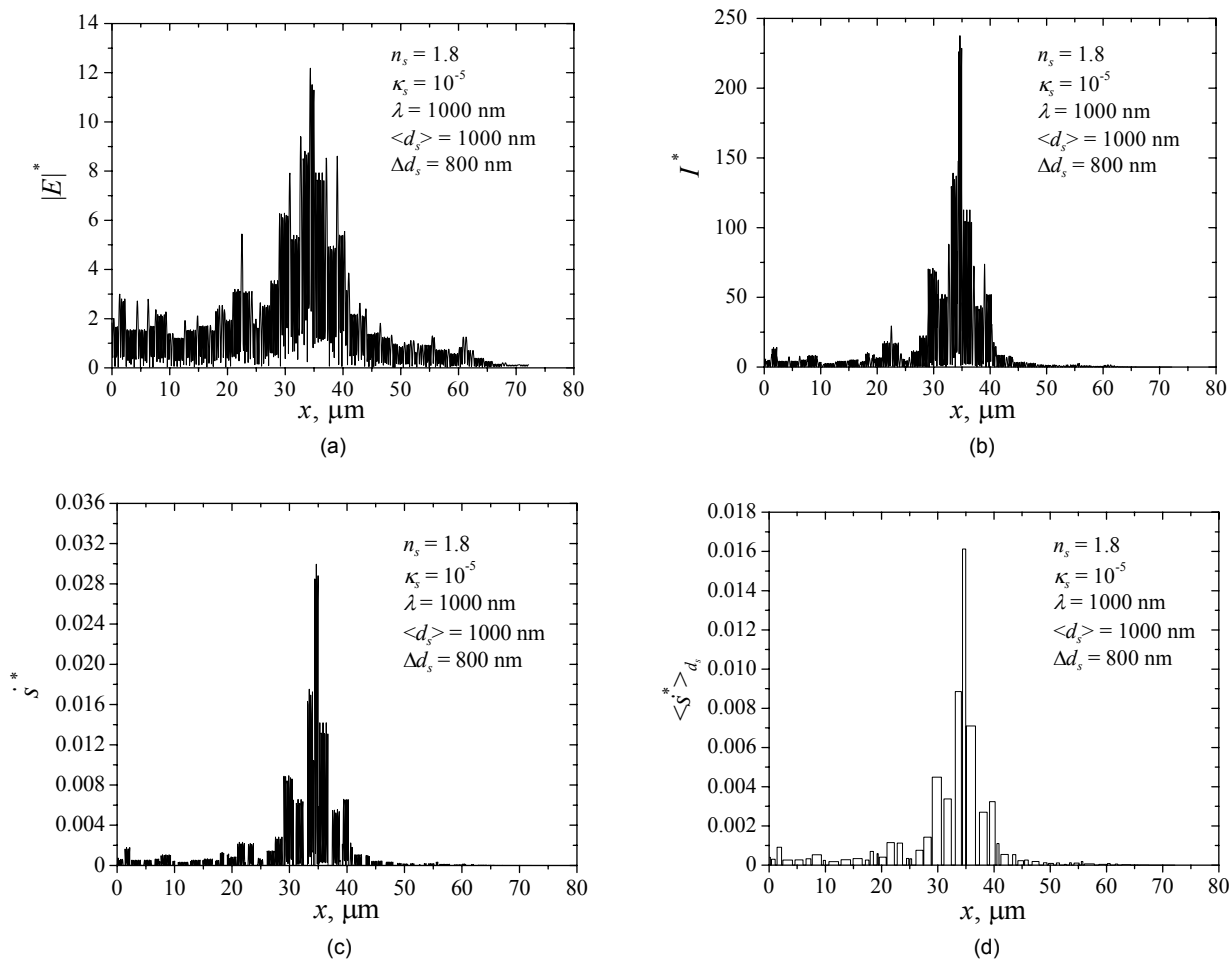

Fig.2 Distributions of the dimensionless (a) field, (b) intensity, (c) volumetric heat generation, and (d) layer averaged volumetric heat generation, for random geometry realization. The porosity is 0.35.

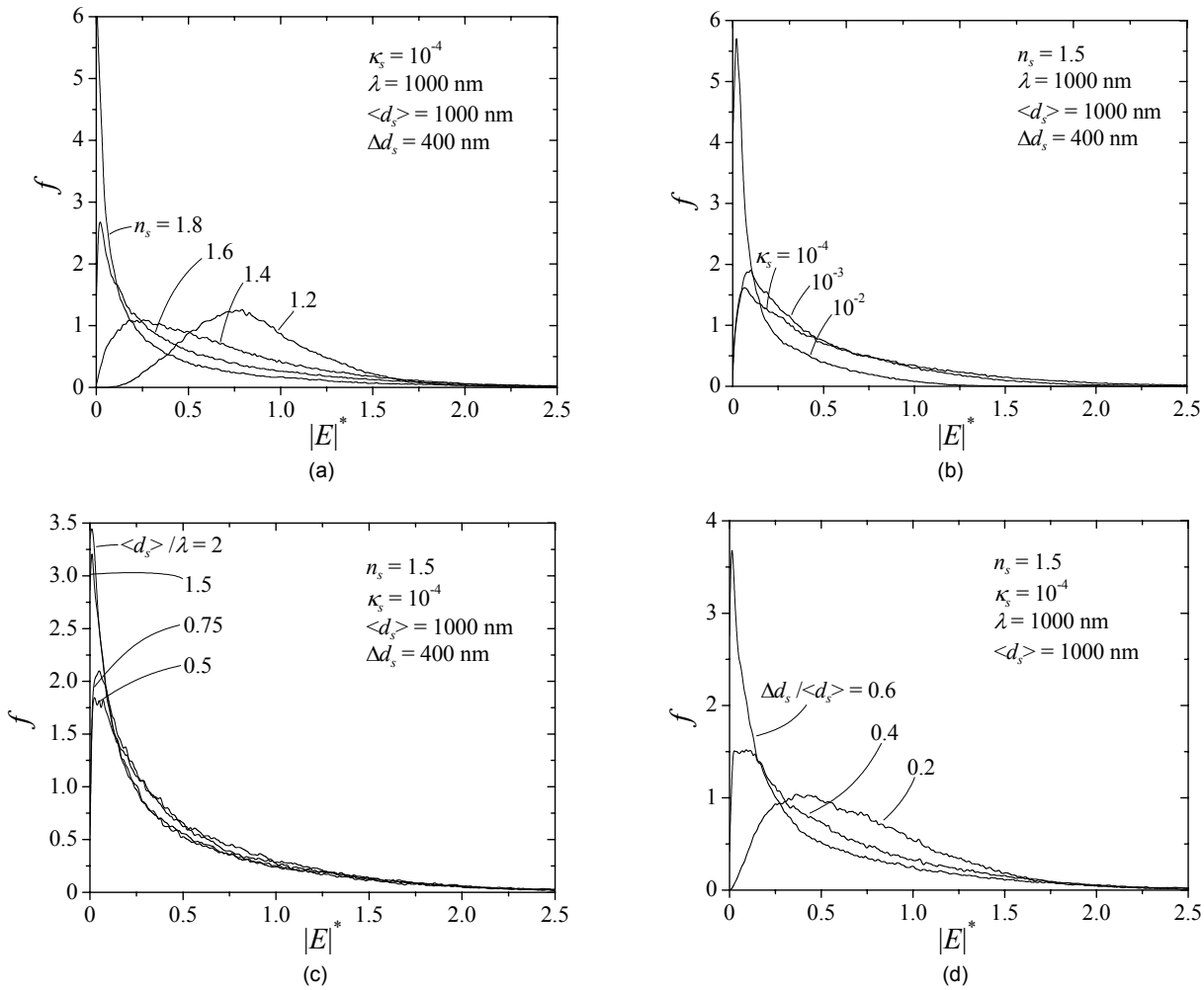

Fig.3. Probability density of occurrence of a field $|E|^*$, within a random porous medium. Effects of solid (a) refractive index, (b) extinction index, (c) size parameter, and (d) size distribution. The porosity is 0.35.

central wavelength λ and a spectrum width $\Delta\lambda$ [11]. In this study we use a monochromatic wave, thus satisfying the coherence condition ($\Delta\lambda$ is 0 and coherence length infinite). The coherence length of many lasers is several km, satisfying the coherence condition.

The individual realizations can also be presented as ensemble averages. We compute N_t = 19,200,000 local-field values $|E|^*$, from N_r = 6,000 different one-dimensional medium realizations, each of which gives N_n = 3,200 field values. From these, we compute the probability density function $f(|E|^*)$. This is found by first dividing all of the field values (from 0 to $|E|^*_{\max}$) into a number of (say N_b) bins (intervals), and then determining the number of field values in each bin. Finally the probability density f_i for the i-th bin is found from

$$f_i = \frac{M_i}{N_t W_b} = \frac{M_i N_b}{N_t |E|^*_{\max}} \ , \qquad (10)$$

where M_i is the number of occurrences in the i-th bin and $W_b = |E|^*_{\max}/N_b$ is the bin width. In our 6,000 realizations, $|E|^*_{\max}$ is 12.2.

The results are shown in Figures 3(a) to (d) for the probability density distribution of $|E|^*$, for several values of refractive index (n_s, κ_s), average layer size ($<d_s>/\lambda$) and the degree of randomness ($\Delta d_s/<d_s>$). As shown in Figures 3(a), (b) and (d), higher values of n_s, k_s and $\Delta d_s/<d_s>$ will result in a higher probability of a smaller $|E|^*$, i.e., there is less probability for field enhancement ($|E|^*>1$). However, Figs. 3(a) and (d) indicate that higher values of n_s and $\Delta d_s/<d_s>$ will favor "extremely large" field enhancement. Figure 3(c) shows that the average size parameter does not affect the field significantly. It should be noted that $|E|^*_{\max}$ was not shown here because of its extremely small probability.

The locations of the field enhancement are determined using the same samplings mentioned above: the N_r = 6,000 different realizations, each of which gives N_n = 3,200 field values at the same set of 3,200 sampling locations. Then for every location x, there are N_r different field values $|E|^*$, some of which (say N_e) are enhanced ($|E|^* > 1$). The probability $p(x)$ of having field enhancement ($|E|^* > 1$) at a location x is found by dividing the number of the occurrences of field enhancement N_e by N_r. This probability is plotted for each of the 3,200 locations, as shown in Fig. 4.

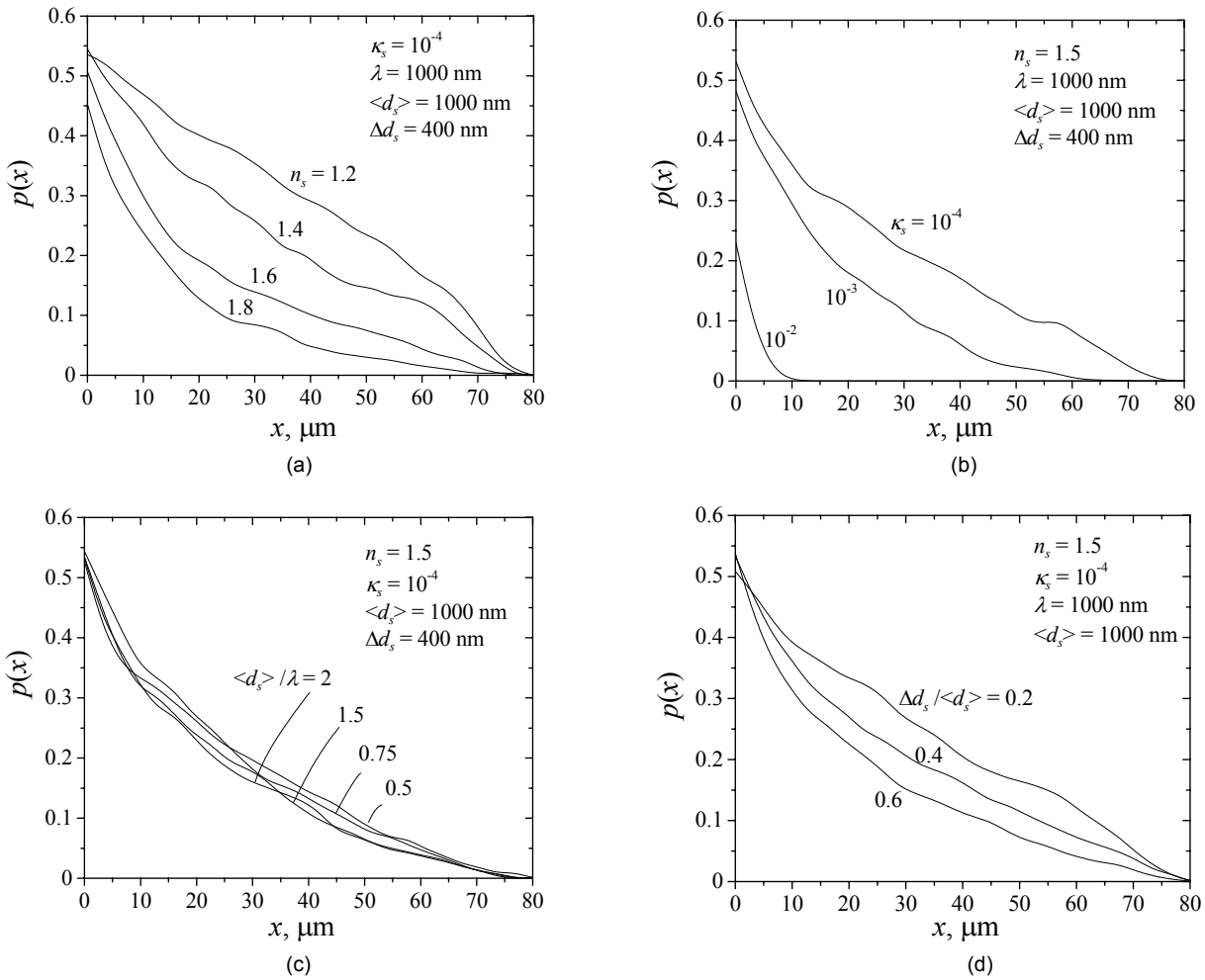

Fig. 4. Probability distribution of field enhancement, for various conditions. Effects of solid (a) refraction index, (b) extinction index, (c) size parameter, and (d) size distribution. The porosity is 0.35.

As shown in Figures 4(a) to (d), fields at the locations closer to the incident surface are always more probable to be enhanced, higher values of n_s, κ_s, $<d_s>/\lambda$ and $\Delta d_s/<d_s>$ will result in less probability of field enhancement.

1.2.2 Comparison of EM Treatment and ERT

It is expected that the ensemble average of the realizations obtained using the Maxwell's equations would result in a behavior predicted by ERT. Here a porous medium model made of 250 composite layers is considered, and 6,000 realizations are used. Note that we use a longer sample than before in order to show more effectively the variation of local intensity with location. Using a same set of 3,200 sampling locations for each realization, we obtain the corresponding 3,200 local-field values for each of the 6,000 different realizations. Then for each of the 3,200 locations, we determine the expected intensity by averaging the 6,000 realizations and the results are shown in Fig. 5, where $<I^*>$ is normalized by the surface values $<I^*>_{x=0}$. The results show that the expected intensity decays exponentially in the direction of wave propagation.

The radiation transport within the same composite can also be treated using ERT. In this treatment, the scattering properties of a single particle are derived first. Then the effective scattering properties are determined for a cluster of particles, using the particle-size distribution. Finally ERT is solved with proper approximations, such as the two-flux model.

For a one-dimensional multilayer media, a layer serves as a single scatterer. For the normal incidence of a planar radiation upon a planar particle, as shown in Fig. 6, the scattering is by reflection.

Using the transfer matrix method, the incident, transmitted and reflected fields are related through

$$\begin{bmatrix} E_i \\ E_r \end{bmatrix} = \begin{bmatrix} \frac{m_s + m_f}{2m_f} & \frac{m_s - m_f}{2m_f} \\ \frac{m_s - m_f}{2m_f} & \frac{m_s + m_f}{2m_f} \end{bmatrix} \begin{bmatrix} e^{ik_s d_s} & 0 \\ 0 & e^{-ik_s d_s} \end{bmatrix} \begin{bmatrix} \frac{m_f + m_s}{2m_s} & \frac{m_f - m_s}{2m_s} \\ \frac{m_f - m_s}{2m_s} & \frac{m_f + m_s}{2m_s} \end{bmatrix} \begin{bmatrix} E_t \\ 0 \end{bmatrix} \tag{11}$$

Thus E_r and E_t are derived in terms of E_i, and the transmission coefficient is a function of the layer thickness d_s, for a given m_f and m_s,

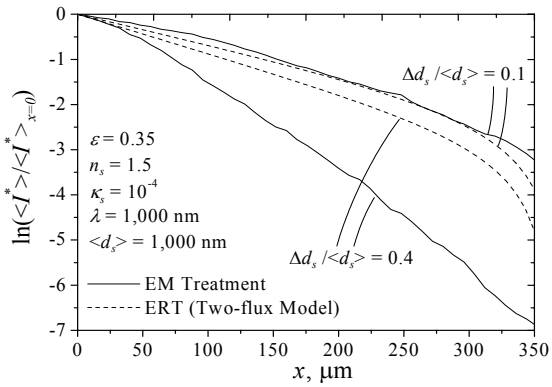

(a)

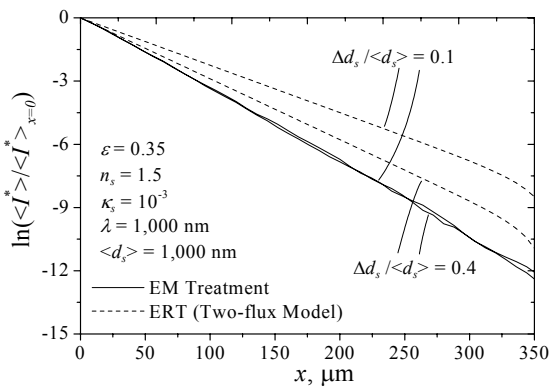

(b)

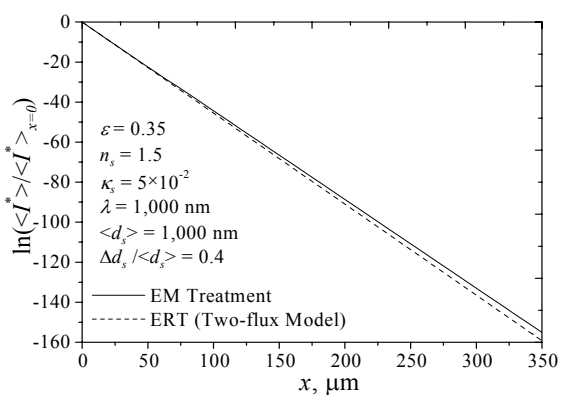

(c)

Fig.5. Distributions of the normalized local intensity for a one-dimensional multilayer porous medium. The EM Treatment (expected values) and ERT (two-flux model) are shown for different particle size distributions. (a) $\kappa_s = 10^{-4}$, (b) $\kappa_s = 10^{-3}$, and (c) $\kappa_s = 5\times10^{-2}$.

$$T_r(d_s) = \frac{I_t}{I_i} = \frac{|E_t|^2}{|E_i|^2}. \tag{12}$$

The extinction coefficient of the single particle is defined as

$$\sigma_e(d_s) = \frac{-\ln T_r(d_s)}{d_s} \tag{13}$$

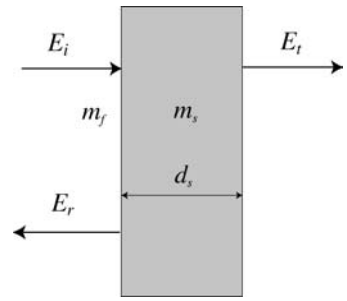

Fig. 6. Transmission and reflection of a single layer

For a random multilayer media of porosity ε, where the layer thickness d_s follows a uniform distribution in the range of $\langle d_s \rangle \pm \Delta d_s$, the effective extinction coefficient becomes

$$\langle \sigma_e \rangle = \frac{\int_{\langle d_s \rangle - \Delta d_s}^{\langle d_s \rangle + \Delta d_s} -\ln T_r(d_s) dd_s}{\int_{\langle d_s \rangle - \Delta d_s}^{\langle d_s \rangle + \Delta d_s} d_s dd_s}(1-\varepsilon). \tag{14}$$

The effective absorption coefficient is

$$\langle \sigma_a \rangle = \frac{4\pi\kappa_s}{\lambda}(1-\varepsilon). \tag{15}$$

Then, the effective scattering coefficient is found from

$$\langle \sigma_s \rangle = \langle \sigma_e \rangle - \langle \sigma_a \rangle. \tag{16}$$

Since scattering occurs only in the backward direction, the scattering phase function is a delta function, i.e.,

$$\Phi(\theta) = \delta(\theta - \pi), \ \int_{-1}^{1} \Phi(\theta) d\cos\theta = 2 \ . \tag{14}$$

The ERT becomes [3]

$$\cos\theta \frac{dI(x,\theta)}{dx} = -\left(\langle \sigma_s \rangle + \langle \sigma_a \rangle\right) I(x,\theta) + \frac{\langle \sigma_s \rangle}{2}\left[\int_0^1 I(x,\theta_i)\Phi(\theta_i - \theta) d\cos\theta_i + \int_{-1}^{0} I(x,\theta_i)\Phi(\theta_i - \theta) d\cos\theta_i\right] . \tag{15}$$

Due to the normal irradiation of a one-dimensional geometry, the radiation field has only two components, namely, forward and backward. Thus the two-flux approximation can be used to solve Eq. (15). By taking $\theta = 0$, and defining $I(x,0) = I^+$, $I(x,\pi) = I^-$, Eq. (15) gives for the forward intensity

$$\frac{dI^+}{dx} = -\left(\langle \sigma_s \rangle + \langle \sigma_a \rangle\right) I^+ + \langle \sigma_s \rangle \left[(1-B)I^+ + BI^-\right] \tag{16}$$

where

$$B = \frac{1}{2}\int_{-1}^{0} \Phi(\theta_i) d\cos\theta_i = 1 \tag{17}$$

Then, Eq. (16) is simplified to

$$\frac{dI^+}{dx} = -\left(\langle\sigma_s\rangle + \langle\sigma_a\rangle\right)I^+ + \langle\sigma_s\rangle I^- \tag{18}$$

Similarly, by taking $\theta = \pi$, Eq. (15) gives for the backward intensity

$$-\frac{dI^-}{dx} = -\left(\langle\sigma_s\rangle + \langle\sigma_a\rangle\right)I^- + \langle\sigma_s\rangle I^+ \quad . \tag{19}$$

The boundary conditions for Eqs.(18) and (19) are $I^+(0) = 1$ and $I^-(L) = 0$, and the solution is

$$I^+ = \frac{(1+\beta^2)\sinh\left[\gamma(L-x)\right] + 2\beta\cosh\left[\gamma(L-x)\right]}{(1+\beta^2)\sinh(\gamma L) + 2\beta\cosh(\gamma L)} \tag{20}$$

$$I^- = \frac{(1-\beta^2)\sinh\left[\gamma(L-x)\right]}{(1+\beta^2)\sinh(\gamma L) + 2\beta\cosh(\gamma L)}, \tag{21}$$

where

$$\beta = \left[\langle\sigma_a\rangle / \left(\langle\sigma_a\rangle + 2\langle\sigma_s\rangle\right)\right]^{\frac{1}{2}} \tag{22}$$

and

$$\gamma = \left[\langle\sigma_a\rangle\left(\langle\sigma_a\rangle + 2\langle\sigma_s\rangle\right)\right]^{\frac{1}{2}}. \tag{23}$$

The local intensity is the sum of the forward and backward intensity

$$I = I^+ + I^- . \tag{24}$$

The predicted distributions of the normalized local intensity are shown in Figs. 5(a)-(c), for κ_s = 10^{-4}, 10^{-3}, and 5×10^{-2}, respectively, and are also compared with the expected results from EM treatment. Both results decay exponentially, but there are differences in the extinction rate, which is inversely rated to the localization length l_{loc}. The results of the EM treatment are for dependent scattering (since the field coherence due to multiple scattering is considered), while those of ERT are for independent scattering. Fig. 5(a) shows that for a weak absorbing solid, the results of the two treatments can be significantly different (for $\Delta d_s / < d_s > = 0.4$), or can be in agreement (for $\Delta d_s / < d_s > = 0.1$). The former is caused by the dependent scattering. As the solid becomes more absorbing, the two results tend to be closer, as shown in Fig. 5(b). For a dominating absorption, i.e., $\langle\sigma_a\rangle >> \langle\sigma_s\rangle$, the two predictions agree very well, as expected.

This indicates that by introducing corrections to the scattering and absorption coefficients, based on the geometric and optical parameters, ERT can represent a statistical behavior of the EM treatment. Two- and three-dimensional fields are computationally more extensive, and this is the main reason for the use of ERT for random porous media. However, ERT masks the significant field enhancement.

2. TWO-DIMENSIONAL GEOMETRY

2.1 Computation

A two-dimensional random porous media used in the computations is shown in Fig. 7. The solids are arranged as an array of infinitely long (in the *y* direction) dielectric cylinders with square section and random size distribution. We again examine the incidence of an electromagnetic wave upon this structure, traveling in the *x*-direction. Due to the complexity of this structure, we seek a numerical solution to the Maxwell's equations using a finite element method based three-dimensional code, High Frequency Structure Simulator (HFSS) [12]. A finite computational domain is chosen, resulting in six surfaces or boundaries. The two *x*-*z* boundaries are treated as periodic boundaries to simulate the infinite length in the *y* direction. The two *x*-*y* boundaries are also treated as periodic boundaries, and the *y*-*z* planes are set to be the incident boundary at $x = 0$ and the radiation boundary at $x = x_0$.

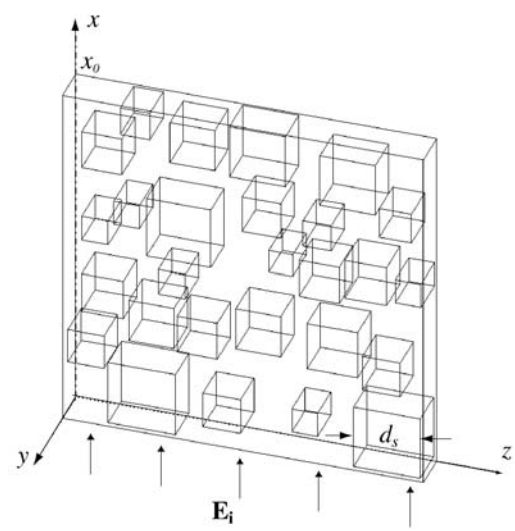

Fig. 7. A two dimensional arrangement of infinitely long square cylinders. The porosity is 0.35.

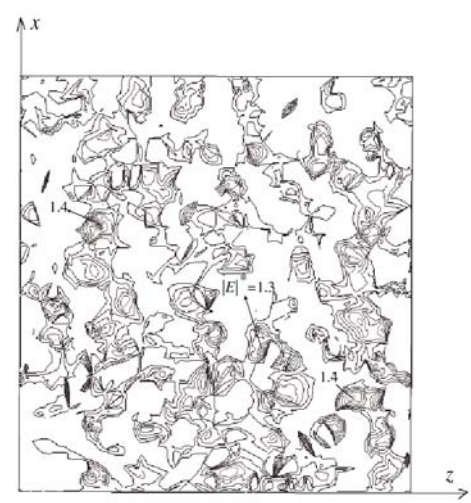

Fig. 8. The two-dimensional distribution of the dimensionless field magnitude $|E|^*$ for the geometry of Fig. 7. The porosity is 0.35.

2.2 Results and Discussions

We choose a computational region of $5\times1\times5$ μm^3. Again, the local electric field in this region is determined for a normal incident electromagnetic wave of wavelength 1000 nm, for a two-dimensional random media with 27 long square cylinders with random linear dimensions $<d_s> \pm \Delta d_s = 1000\pm400$ nm, and with $n_s = 1.8$ and $\kappa_s = 10^{-5}$ in air. The results are shown in Fig. 8, using contours of constant dimensionless electric field. Similar to the one-dimensional results, there is field enhancement within the random porous medium. However, based on the limited number of realizations we used for computation, the extent of enhancement in two-dimensional structures is smaller ($|E|^*$ is less than 2). This is due to the lower probability of having coherent superposition of the scattered waves. In the one-dimension geometry, the scattering is limited to forward and backward directions, while in the two-dimensional geometry, the scattering is distributed over 2π (although not uniformly).

3. CONCLUSIONS

In monochromatically irradiated, one- and two-dimensional dispersed dielectric solids with random non-uniform size distribution, solutions of the Maxwell's equations indicate that there is a field enhancement which can be one order larger of magnitude than the incident field, for some arrangements. The probability of enhanced $|E|^*$ and its locations of this enhancement are influenced by the solid complex refractive index and particle size distribution. Using individual realizations as well as their ensemble averages, it is shown that ERT, by introducing corrections to the scattering and absorption coefficients based on dependent scattering, is a statistical average of the EM treatment, so it is not suitable for the prediction of any field enhancement and photon localization.

ACKNOWLEDGMENTS

The collaboration and assistance of Professor Steven Rand and Mr. Shawn Redmond of the Department of Electrical Engineering and Computer Science and the Applied Physics Program, University of Michigan, are greatly appreciated.

REFERENCES

[1] Redmond, S., Rand, S.C., Ruan, X.L., and Kaviany, M., "Multiple Scattering and Nonlinear Thermal Emission of Yb3+,Er3+:Y_2O_3 Nanopowders", Journal of Applied Physics, submitted.

[2] Rand, S.C., 2003. "Bright storage of light". Optics and Photonics News, May, pp. 12-17.

[3] Kaviany, M., 1995. *Principles of Heat Transfer in Porous Media, Second Edition*. Springer, New York.

[4] Tanaka, K. and Tanaka, M., 1997. "Is ball lightning "Anderson Localization"?: Localized and enhanced fields in a corridor with irregular-shaped metal walls". Appl. Phys. Lett., **71**, pp. 3793-3795.

[5] McGurn, A.R., Christensen, K.T., Mueller, F.M., and Maradudin, A.A., 1993. "Anderson localization in one-dimensional randomly disordered optical systems that are periodic on average". Physical Review B,, **47**, pp. 13120-13125.

[6] Yoo, K.M. and Alfano, R.R., 1989. "Photon localization in disordered multilayer system". Physical Review B, **39**, pp. 5806-5809.

[7] Knittl, Z., 1976. *Optics of thin films; an optical multilayer theory*. Wiley, New York.

[8] Hayt, W.H. and Buck, J.A., 2001. *Engineering electromagnetics, sixth edition*. McGraw-Hill, Boston.

[9] Sigalas, M.M., Soukoulis, C.M., Chan, C._T., and Turner, D., 1996. "Localization of electromagnetic waves in two-dimensional disordered systems". Physical Review B, **53**, pp. 8340-8348.

[10] Pendr, J.B., and Mackinnon, A., 1992. "Calculation of photon dispersion relations". Physical Review Letters, **69**, pp. 2772-2775.

[11] Hecht, E., 2002. *Optics*. Addison Wesley, San Francisco.

[12] Ansoft Corp., 2001. *High Frequency Structure Simulator, Getting Started: An Antenna Problem*.